Materials Today Bio 16 (2022) 100411

Contents lists available at ScienceDirect

Materials Today Bio

journal homepage: www.journals.elsevier.com/materials-today-bio

Shape-controllable and kinetically miscible Copper–Palladium bimetallic nanozymes with enhanced Fenton-like performance for biocatalysis

Wensheng Xie [a], Genpei Zhang [b,c], Zhenhu Guo [d], Hongye Huang [a], Jielin Ye [d], Xiaohan Gao [d], Kai Yue [b,c], Yen Wei [a,*], Lingyun Zhao [d,**]

[a] The Key Laboratory of Bioorganic Phosphorus Chemistry & Chemical Biology (Ministry of Education), Department of Chemistry, Tsinghua University, Beijing 100084, PR China
[b] School of Energy and Environmental Engineering, University of Science and Technology Beijing, Beijing 100083, PR China
[c] Shunde Graduate School of University of Science and Technology Beijing, Shunde, Guangdong Province, 528399, PR China
[d] State Key Laboratory of New Ceramics and Fine Processing, School of Materials Science and Engineering, Tsinghua University, Beijing 100084, PR China

ARTICLE INFO

Keywords:
Palladium
Copper
Bimetallic nanozymes
Fenton-like reaction

ABSTRACT

Bimetallic nanozymes have been emerging as essential catalysts due to their unique physicochemical properties from the monometallics. However, the access to optimize catalytic performance is often limited by the thermodynamic immiscibility and also heterogeneity. Thus, we present a one-step coreduction strategy to prepare the miscible Cu–Pd bimetallic nanozymes with controllable shape and homogeneously alloyed structure. The homogeneity is systematically explored and luckily, the homogeneous introduction of Cu successfully endows Cu–Pd bimetallic nanozymes with enhanced Fenton-like efficiency. Density functional theory (DFT) theoretical calculation reveals that Cu–Pd bimetallic nanozymes exhibit smaller d-band center compared with Pd nanozymes. Easier adsorption of H_2O_2 molecular contributed by the electronic structure of Cu significantly accelerate the catalytic process together with the strong repulsive interaction between H atom and Pd atom. *In vitro* cytotoxicity and intracellular ROS generation performance reveal the potential for *in vivo* biocatalysis. The strategy to construct kinetically miscible Cu–Pd bimetallic nanozymes will guide the development of bimetallic catalysts with excellent Fenton-like efficiency for biocatalytic nanomedicine.

1. Introduction

Bimetallic nanoparticles have attracted broad attentions due to the unique catalytic properties in various fields, especially in chemical sensing, heterogeneous catalysis, and nanomedicine [1–3]. Different from monometallic nanoparticles, bimetallic nanoparticles always present unique multifunctional performances due to the synergistic effects among of corresponded monometallic analogues [4]. For instance, Cu–Ni bimetallic nanoparticles have been obtained via nonequilibrium synthetic strategy and exhibit enhanced C_{2+} product Faradaic efficiencies (~76%), which is ~20% higher than that of monometallic Cu [5]. Yang and coworkers have precisely explored the activity of Au–Cu bimetallic nanoparticles as a function of their composition and demonstrated that uniform Au_3Cu bimetallic nanoparticles exhibit highest catalytic activity, while pure Cu nanoparticles owned the lowest overall activity [6]. Compared to monometallic materials, the design and development of bimetallic nanoparticles greatly optimize the functionality and broaden the applications.

Due to the fact that various factors like size, morphology, component, and nanoscale arrangement will influence the physicochemical properties, many research interests have been paid to deliberately identify the relationship between enhanced catalytic performances and structures in order to expand the practical applications in the field of catalysis [7,8]. However, there still remains two fundamental challenges: the limited access to obtain homogeneously alloyed bimetallic nanozymes due to the thermodynamic immiscibility and the difficulty to identify and optimize the catalytic performance because of the heterogeneity in bimetallic catalysts [5]. Traditional preparation methods such as seed-mediated growth, galvanic replacement, concurrent thermal decomposition, and impregnation tend to yield bimetallic nanozymes with unfavorable structures, broad size distributions, inhomogeneous alloying, and other heterostructures [2,9]. New methods like surface plasmon resonance

* Corresponding author.
** Corresponding author.
E-mail addresses: weiyen@mail.tsinghua.edu.cn (Y. Wei), lyzhao@tsinghua.edu.cn (L. Zhao).

https://doi.org/10.1016/j.mtbio.2022.100411
Received 8 July 2022; Received in revised form 23 August 2022; Accepted 24 August 2022
Available online 15 September 2022

[10] and pulsed laser ablation [11,12] always require complex processes and extreme conditions. Although J. R. Regalbuto and coworkers have successfully obtained highly dispersed, well-alloyed bimetallic ~1 nm-diameter nanoparticles via strong electrostatic adsorption, the strategy dependents on the oppositely charged oxide or carbon supports [7]. Thus, it is of great significance to construct bimetallic nanozymes with homogeneously alloyed structure and optimized catalytic properties [13].

Herein, to optimize the Fenton-like performance of Pd-based nanozymes, in this study, a one-step coreduction strategy was employed to prepare miscible Cu–Pd bimetallic nanozymes (alliums-like $CuPd_3$ nanozyme, and concave rhombic dodecahedral-like Cu_3Pd) with controllable shape and homogeneously alloyed structure. The synthetic procedure lasts only 2 h under 110 °C by using Na_2PdCl_4 and $CuCl_2$ as precursors in the presence of hexadecylamine (HDA) and glucose. We firstly systematically investigated the morphologies, structures, and atomically spatial states of as-synthesized Cu–Pd bimetallic nanozymes. Then the optimal catalytic activities, kinetics, and ROS products were carefully evaluated by adjust the molar ratio of precursors. To disclose the mechanism of optimal Fenton-like efficiency, the density functional theory (DFT) theoretical calculation was performed to explore the total reaction energy, density of state, and d-band center. Finally, the *in vitro* cytotoxicity and intracellular ROS generation performance were evaluated to reveal the potential for *in vivo* biocatalysis. It is believed that this research will guide the development of homogeneous Cu–Pd bimetallic nanozymes with excellent Fenton-like efficiency for biocatalytic nanomedicine.

2. Materials and methods

2.1. Materials

Sodium tetrachloropalladate (II) (Na_2PdCl_4), cupric chloride dehydrates ($CuCl_2{\cdot}2H_2O$), glucose, and hexadecylamine (HDA) were purchased from Sigma-Aldrich LLC. Ethanol and deionized water were obtained from Beijing Chemical Industry Group Corporation Co., Ltd. Copper (II) phthalocyanine (CuPc) was brought from Zancheng (Tianjin) Technology Co., Ltd. TMB (3,3′,5,5′-Tetramethylbenzidine) Single-Component Substrate Solution, CCK-8 Cell Proliferation and Cytotoxicity Assay Kit, and 2′,7′-Dichlorofluorescin Diacetate (DCFH-DA) fluorescent probe were obtained from Solarbio Life Sciences & Technology Co., Ltd. All chemicals were employed without further purification.

2.2. Characterization

Transmission electron microscopy (TEM, HT-7700, Hitachi) and high-resolution transmission electron microscopy (HRTEM, JEM-2100F, JEOL) with energy dispersive X-ray (EDX) spectroscopy were used to explore the morphology, crystal structure, and element components of as-synthesized Pd and Cu–Pd bimetallic nanozymes. The size distribution and zeta potential in aqueous solution were measured on Malvern Zetasizer Nano ZS. The aberration-corrected high-angle annular dark-field scanning TEM (AC HAADF-STEM, FEI Titan Cubed G2 300) was performed to obtain the high-resolution AC HAADF-STEM images of Pd and Cu–Pd bimetallic nanozymes at 300 keV. X-ray diffractometer (XRD, D/max-2550, Rigku) was used to analyze the crystal structure of powder. XPS spectra of samples were measured on the X-Ray Photoelectron Spectroscopy (250XI, Thermo Fisher Scientific). The electron spin resonance (ESR) spectra were trapped by 5,5-dimethyl-1-pyrroline N-oxide (DMPO) in aqueous solution with Cu_3Pd, $CuPd_3$, and Pd (10 μg/mL). The intracellular GSSG level was measured by GSH and GSSG Assay Kit.

2.3. Preparation of Cu–Pd bimetallic nanozymes

Hovenia acerba-like Pd nanozymes: 2.67 mL Na_2PdCl_4 aqueous solution (122.4 mM) and 200 mg HDA were added into 7 mL ultrapure (UP) water in a 20 mL Wheaton Sample Vial. The mixture was magnetically stirred overnight at ambient temperature for complete dissolution. Then, the solution was transferred into a 100 mL round-bottom flash and another 1 mL glucose aqueous solution (75.7 mM) was added. The system was heated to 110 °C for 2 h under magnetic stirring. After cooling down to room temperature, the product was washed with aqueous ethanol solution (20 vol%) for four times and redispersed in 2 mL UP water for further use.

Cu–Pd bimetallic nanozymes: Following the same strategy as Pd nanozymes, alliums-like $CuPd_3$ nanozymes were prepared by adding 0.42 mL $CuCl_2$ H_2O aqueous solution (100 mM) at the beginning, and concave rhombic dodecahedral-like Cu_3Pd nanozymes were prepared by synchronously adding 1.24 mL $CuCl_2$ H_2O aqueous solution (100 mM).

2.4. Fenton-like efficiency and kinetics measurement

In order to evaluate the Fenton-like efficiency and kinetics performance, TMB Single-Component Substrate Solution was employed to detect the generated hydroxide radical (OH) as protocol in our previous study. For testing Cu–Pd bimetallic nanozymes concentration-dependent kinetics, 0.5 mL TMB Single-Component Substrate Solution and 0.5 mL UP water were mixed in a 48-well plate firstly. Then Cu–Pd bimetallic nanozymes were added for a final concentration of 500, 200, 100, and 50 μg/mL quickly. The time-dependent absorbance value at 652 nm was detected in a Microplate Reader (Varioskan LUX, Thermo Scientific). The UV–vis spectra of above mixture were measured when the reaction lasts for 0.5 h. Besides, for measuring H_2O_2 concentration-dependent kinetics, additional H_2O_2 was added into the TMB Single-Component Substrate Solution for a final H_2O_2 concentration of 40, 30, 20, 10, 5, 1 mM. The time-dependent absorbance value at 652 nm was detected immediately after Pd and Cu–Pd bimetallic nanozymes were added (Pd: 300 μg/mL, $CuPd_3$: 300 μg/mL, Cu_3Pd: 150 μg/mL). Meanwhile, the UV–vis spectra of Cu–Pd bimetallic nanozyme in various TMB/H_2O_2 solution (H_2O_2 concentration: 40, 30, 20, 10, 5, 1 μM) were measured when the reaction lasts for 0.5 h.

2.5. X-ray absorption spectrum measurement

For X-ray absorption spectrum measurement, Cu–Pd bimetallic nanozyme powders were prepared via lyophilization strategy. Cu K-edge X-Ray absorption spectra (XAS) data of Cu–Pd bimetallic nanozyme were collected on beam line Si(111) crystal monochromators at the BL11B beamlines at the Shanghai Synchrotron Radiation Facility (SSRF) (Shanghai, China). X-ray absorption near-edge structure (XANES) was observed between two scans taken for a specific sample and extended X-ray absorption fine structure (EXAFS) data were performed by in transmission mode. The data were analyzed by the software of Athena. Wavelet Transform (WT) was carried out with hamaFortran software.

2.6. DFT theoretical calculation

The structural files of Cu (111) and Pd (111) were downloaded from AMCSD (American Mineralogist Crystal Structure Database). The substitutional atoms were set, and three metal-organic models were created by GaussView5.0, which had 16 transition metal atoms and two hydrogen peroxide molecules. The optimizations of the systems were carried out by using PBE method and LANL2TZ basis set as employed in Gaussian 16 package. Then the equilibrations in a constant ensemble (NPT) for a duration of 2 ps and the molecular dynamics (MD) simulations with 200 ps in a canonical ensemble (NVT) were performed by using GFN2-XTB method in the CP2K package, of which the temperature was 310 K and the pressure was 1 bar. Density of States (DOS) analysis has also been obtained by MULTIWFN 3.8 program, and d-band center was calculated to study the adsorption between the transition metal surface and hydrogen peroxide (H_2O_2).

2.7. In vitro cytotoxicity evaluation

To evaluate the *in vitro* cytotoxicity of as-synthesized Pd and Cu–Pd bimetallic nanozyme, 4T1 murine mammary cancer cell line was chosen as model. In detail, cells in exponential phase were seeded in a 96-well plate with a concentration of 5000/well. 12 h later, the medium was replaced with fresh medium (various Pd and Cu–Pd bimetallic nanozyme: 400, 200, 100, 50, 25, 12.5, 6.25, 0 μg/mL). After another 24 h incubation, the cell viability of 4T1 cells was measured by cell count kit-8 (CCK-8).

2.8. Intracellular hydroxide radical detection

DCFH-DA fluorescent probe was employed to detect the intracellular OH catalyzed by Pd and Cu–Pd bimetallic nanozymes. In general, 4T1 cells in exponential phase were seeded in a 96-well plate with a concentration of 5000/well. 12 h later, the medium was replaced with fresh medium with Pd and Cu–Pd bimetallic nanozymes concentration of 25 μg/mL. After incubation for another 6 h, the Pd and Cu–Pd bimetallic nanozymes were removed thoroughly and the cells were stained with DCFH-DA probe. Finally, confocal laser scanning microscopy (FV3000, Olympus) was used to image the cells with excitation/emission wavelength: 504/529 nm.

2.9. Statistical analysis

Results in this study were presented as mean values ± SD, and the statistical difference was calculated by two-tailed student's *t*-test. *$p < 0.05$, **$p < 0.01$, ***$p < 0.001$.

3. Results and discussion

3.1. Synthesis and characterization of Pd and Cu–Pd bimetallic nanozymes

As illustrated in Fig. 1a, the one-step coreduction strategy was introduced to prepare the hovenia acerba-like Pd nanozyme and Cu–Pd

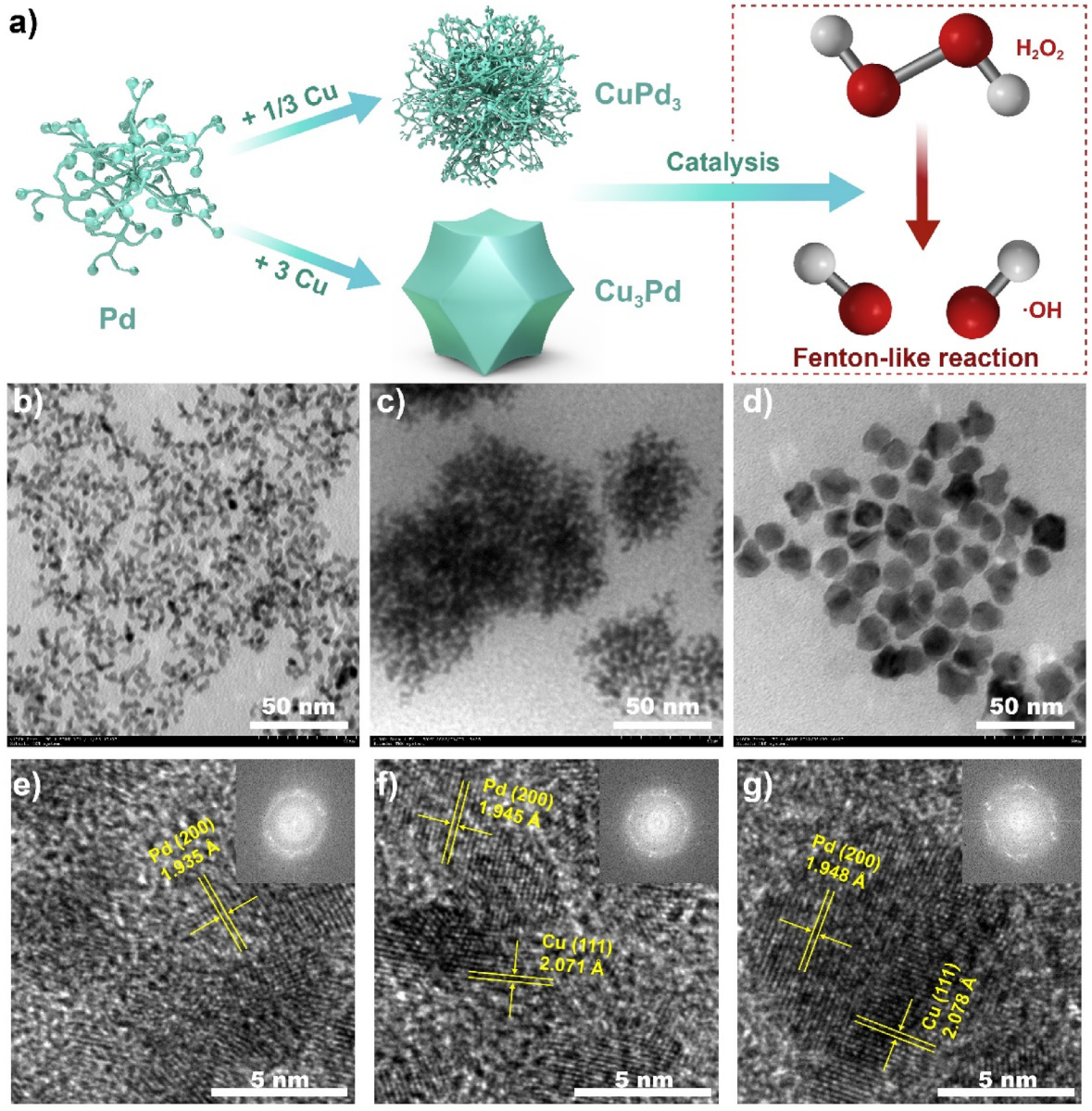

Fig. 1. Synthesis and basic characterization of Pd and Cu–Pd bimetallic nanozymes. (a) Schematical illustration of Pd and Cu–Pd bimetallic nanozymes synthetic procedure and Fenton-like reaction activity. (b–d) TEM images of Pd (b), $CuPd_3$ (c), and Cu_3Pd (d). (e–g) HRTEM images of Pd (e), $CuPd_3$ (f), and Cu_3Pd (g).

bimetallic nanozymes (alliums-like $CuPd_3$ nanozyme, and concave rhombic dodecahedral-like Cu_3Pd) for optimized Fenton-like efficiency (catalyzing H_2O_2 into hydroxide radical (OH)). Generally, Na_2PdCl_4 and $CuCl_2{\cdot}2H_2O$ were employed as metal precursors and glucose was taken as reductant during the one-pot preparation procedures in the presence of hexadecylamine (HDA). By adjusting the molar ratio of Pd and Cu precursor, homogeneously alloyed Cu–Pd bimetallic nanozymes with different morphology and structure were obtained. As shown in Fig. 1b, the transmission electron microscopy (TEM) image of Pd nanozyme presents regular and homogeneous hovenia acerba-like structure with a narrow size distribution. When 1/3 M ratio of Cu/Pd precursor was added, the obtained $CuPd_3$ nanozyme exhibits agminated and pyknotic alliums-like structure (Fig. 1c). Furthermore, a concave rhombic dodecahedral-like structure (Fig. 1d) appears when the molar ratio of Cu/Pd precursor increases to 3. High-resolution transmission electron microscopy (HRTEM) images of Pd and Cu–Pd bimetallic nanozymes

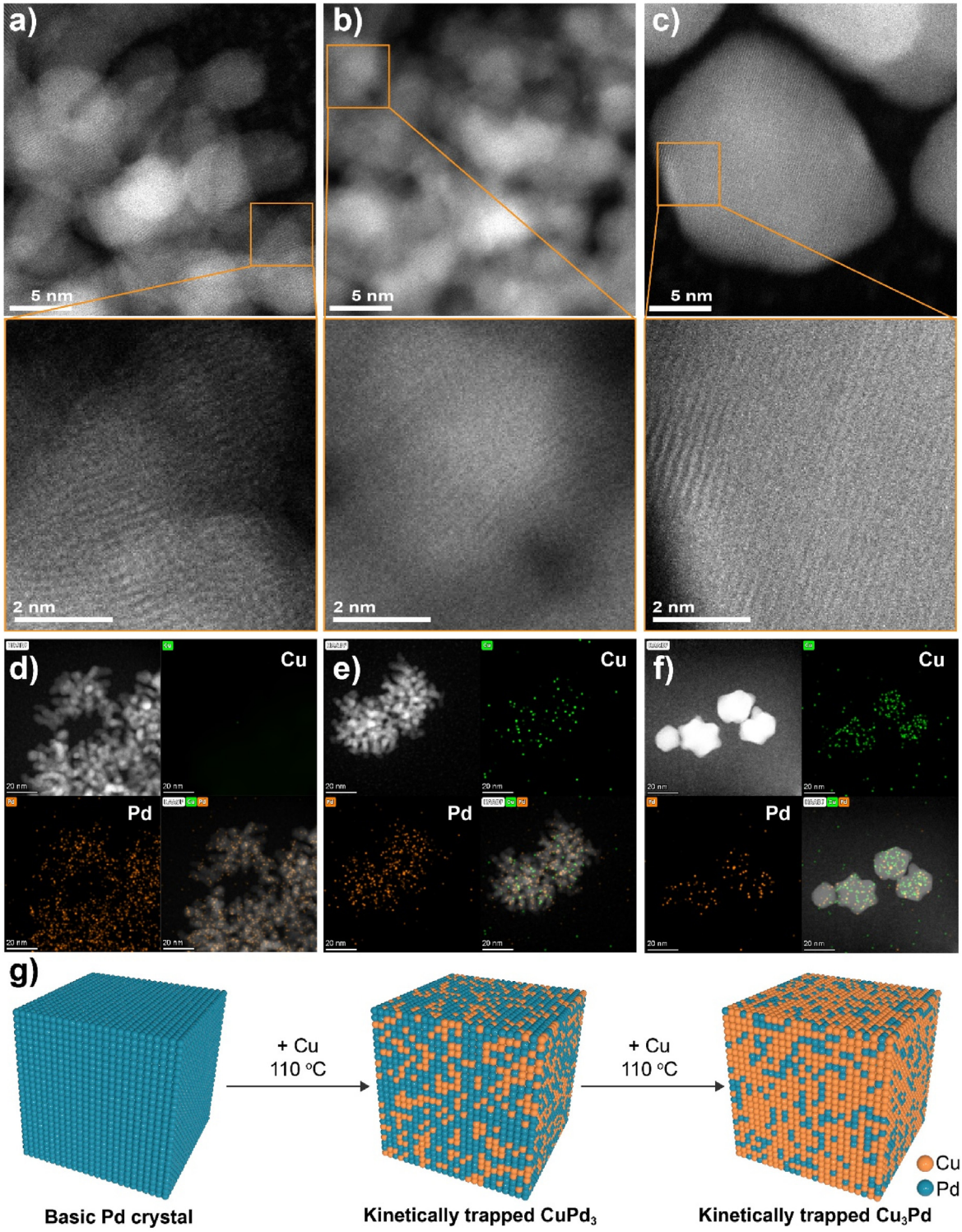

Fig. 2. (a–f) AC-HAADF-STEM images of Pd (a), $CuPd_3$ (b), and Cu_3Pd (c). (d–f) Corresponding element mapping (HADDF image, Cu, Pd, merge image) of Pd (d), $CuPd_3$ (e), and Cu_3Pd (f). (g) Atomistic simulation scheme describes the formation of kinetically trapped homogeneous Cu–Pd bimetallic nanozymes.

clearly demonstrate the fine crystal structure with periodic fringe spaces (Fig. 1e–g). As presented in Fig. 1e, the d-spacing value is measured to be 1.935 Å, which is consistent with the d-spacing value for (200) of pure Pd nanozyme. Meanwhile, the d-spacing of 2.071 Å, and 2.078 Å for $CuPd_3$ nanozyme (Fig. 1f) reveals the lattice plane of Cu (111) and Pd (200), respectively. The same lattice planes are also detected for Cu_3Pd nanozyme at d-spacing of 2.078 Å and 1.948 Å, indicating the fine crystal structure of Cu–Pd bimetallic nanozymes. As-synthesized Pd and Cu–Pd bimetallic nanozymes show excellent dispersibility and stability in water, phosphate buffer saline (PBS), and DMEM medium (Fig. S1). The size distribution obtained by dynamic light scattering (Fig. S2) is consistent with TEM images and all of them demonstrate negative zeta potential (Fig. S3). Besides, X-ray diffraction (XRD) was performed to explore the crystal structure of as-prepared Cu–Pd bimetallic nanozymes. The XRD

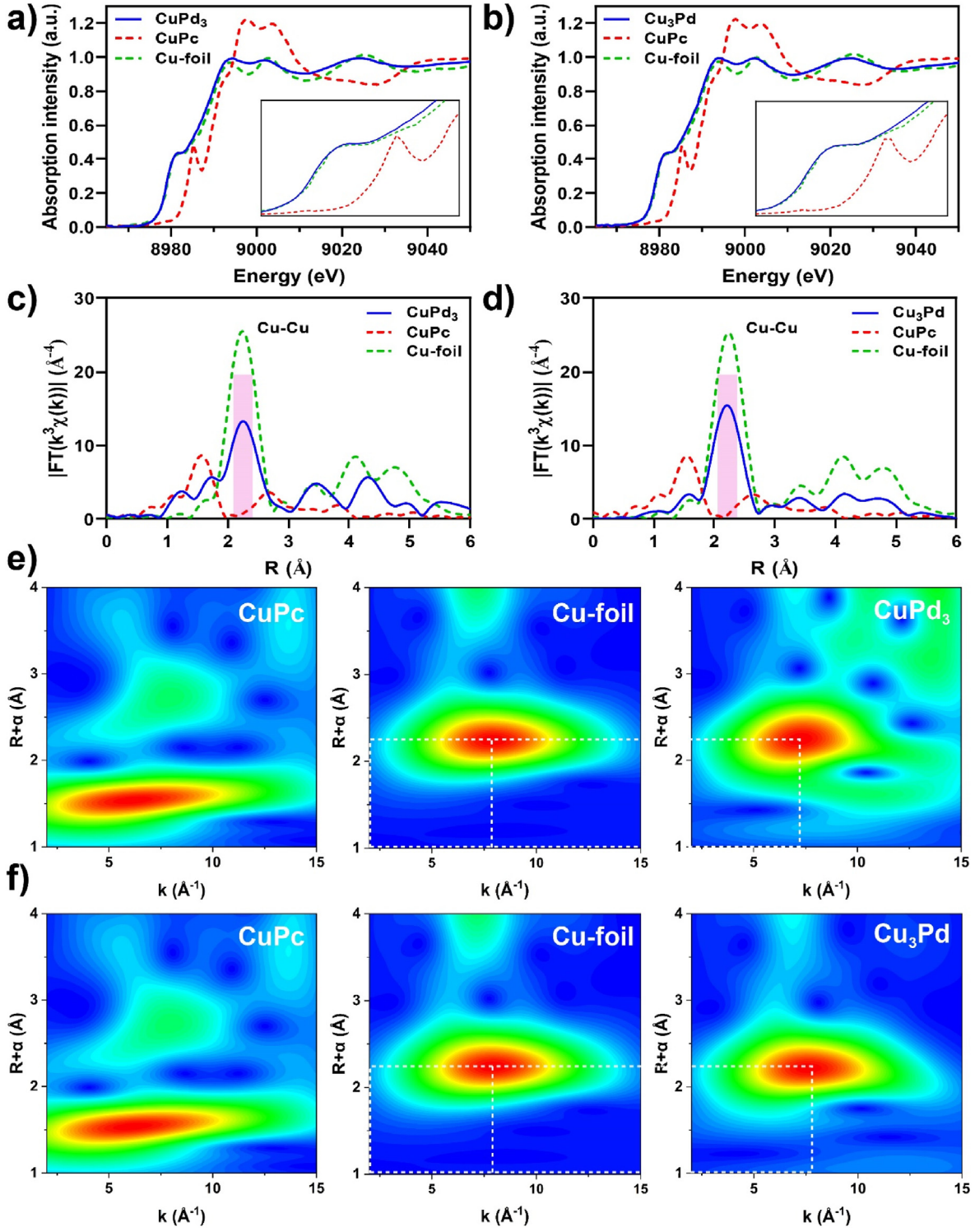

Fig. 3. X-ray absorption evaluation for Cu–Pd bimetallic nanozymes. (a, b) XANES and magnified pre-edge XANES spectra taken at Cu K-edge of $CuPd_3$ (a) and Cu_3Pd (b). (c, d) Fourier transform of Cu-edge EXAFS of $CuPd_3$ (c) and Cu_3Pd (d) in R-space. (e, f) Wavelet Transform image at the Cu-edge of $CuPd_3$ (e) and Cu_3Pd (f). Cu-foil and CuPc were taken as reference.

pattern in Fig. S4a shows the characteristic peaks of Pd at about 40.1° for (111), 46.7° for (200), and 68.1° for (220), which is consistent with the standard PDF card (PDF#46–1043). For the samples were loaded by a transparent glass slide, the strong peak at about 21.6° is responsible for the (111) of silicon dioxide (PDF#27–0605). The XRD pattern of $CuPd_3$ (Fig. S4b) and Cu_3Pd (Fig. S4c) nanozymes present obvious diffraction peak shifting to high angle positions, indicating the increasing doping amount of Cu in Pd lattice. Meanwhile, the characteristic peaks of (111), (200), and (220) of Cu at about 43.3°, 50.4°, and 74.1° appear (PDF#04–0836), demonstrating that cubic crystal system of Cu become the main phase. It is well known that Cu and Pd have the same crystal system (cubic), similar space group (Fm-3m and Fd-3m), and approximately equal atomic diameter (1.28 Å and 1.37 Å), which making it easy to form the homogenous Cu–Pd bimetallic nanozymes [5]. According to the Cu–Pd binary phase diagrams (Fig. S5), there are two superlattices ($L1_2$ and B_2) for the low-temperature ordered phases [14,15]. And the $L1_2$ structure is the ordered phase Cu_3Pd with a composition range of homogeneity.

In order to further study the atomic spatial information of Cu and Pd (single-atom or intermetallic compound), we tested the Pd and Cu–Pd nanozymes using the high-angle-annular-dark-field scanning transmission electron microscopy (HAADF-STEM) (Fig. 2a–c). Compared with the HAADF-STEM images of pure Pd nanozyme (Fig. 2a), there is no evident nanoparticle and metallic cluster in both $CuPd_3$ (Fig. 2b) and Cu_3Pd (Fig. 2c) nanozymes, indicating the homogenous alloying of Cu and Pd, which is consistent with the results of element mapping. Meanwhile, none small bright/dark dots appear in the aberration-corrected HAADF-STEM (AC-HAADF-STEM) images with sub-Angstrom resolution of $CuPd_3$ (Fig. 2b) and Cu_3Pd (Fig. 2c) nanozymes, demonstrating the spacing state of Cu and Pd atom in lattice is not single-atom, but intermetallic compound. The simultaneously obtained energy-dispersive X-ray spectroscopy (EDS) spectra (Figs. S6a–c) confirms the presence of Cu and Pd in $CuPd_3$ and Cu_3Pd nanozymes. To intuitively verify the successful synthesis of Pd and Cu–Pd bimetallic nanozymes, the EDS mapping on HRTEM was carried out (Fig. 2d–f). The results clearly exhibit the pure Pd nanozyme and the homogenous distribution of Cu

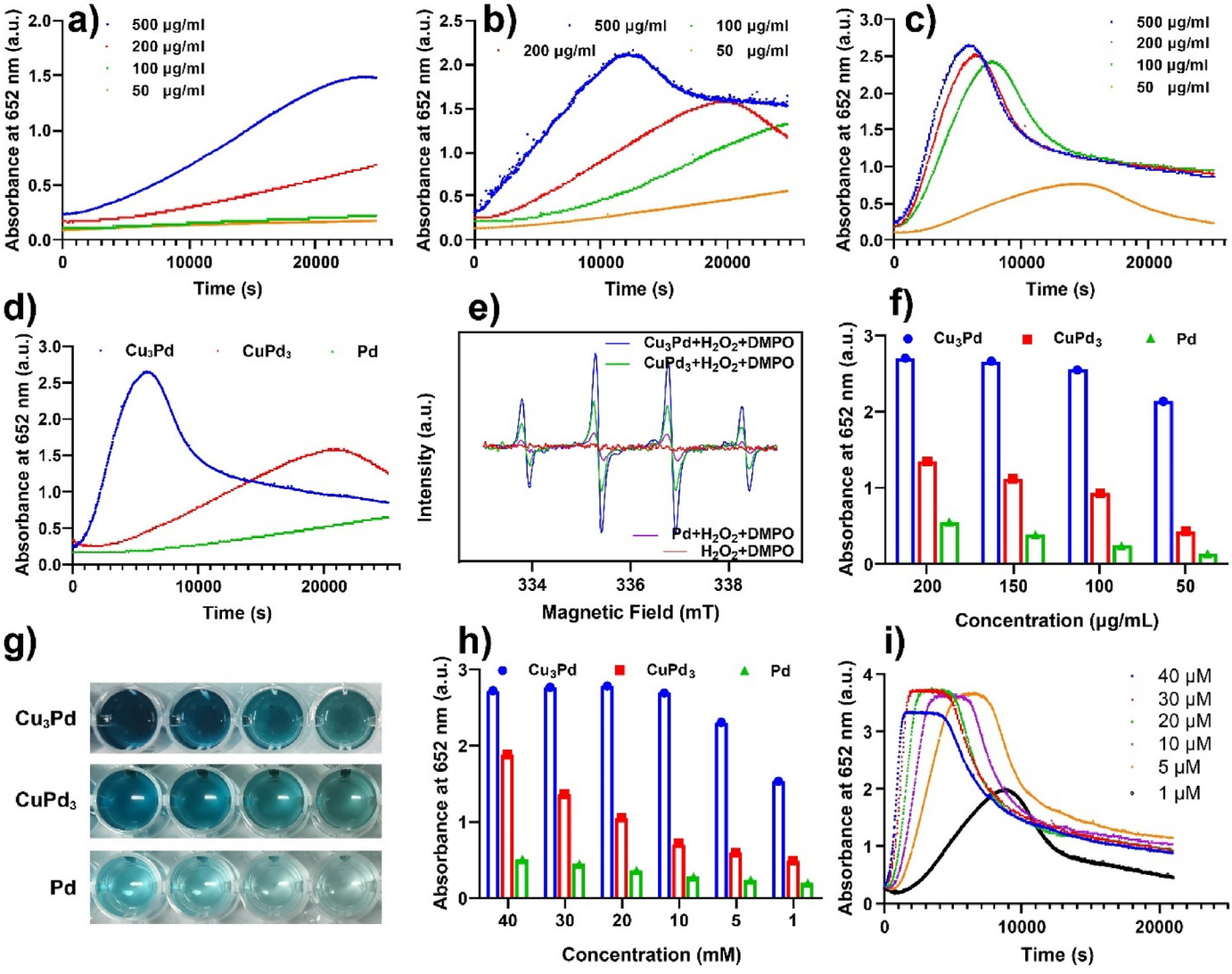

Fig. 4. Fenton-like reaction activity and kinetics performance of Cu–Pd bimetallic nanozymes. (a-c) Time-dependent UV–vis absorbance of Cu_3Pd (a), $CuPd_3$ (b), and Pd (c) in TMB/H_2O_2 solution with various concentrations (500, 200, 100, 50 μg/mL). (d) Time-dependent UV–vis absorbance of Cu–Pd bimetallic nanozymes in TMB/H_2O_2 solution with concentration of 200 μg/mL (e) ESR spectra of hydroxide radical trapped by 5,5-dimethyl-1-pyrroline N-oxide (DMPO) in aqueous solution with Cu_3Pd, $CuPd_3$, and Pd (10 μg/mL). (f) UV–vis absorbance value at 652 nm of TMB/H_2O_2 solutions after incubation with Cu–Pd bimetallic nanozymes (200, 150, 100, 50 μg/mL) for 1.5 h. (g) Photographs of TMB/H_2O_2 solutions after incubation with Cu–Pd bimetallic nanozymes (500, 200, 100, 50 μg/mL) for 1.5 h. (h) UV–vis absorbance value at 652 nm of TMB/H_2O_2 solutions (H_2O_2 concentration: 40, 30, 20, 10, 5, 1 mM) after incubation with Cu–Pd bimetallic nanozymes for 0.5 h. (i) Time-dependent UV–vis absorbance of Cu_3Pd in various TMB/H_2O_2 solution (H_2O_2 concentration: 40, 30, 20, 10, 5, 1 μM).

and Pd in both $CuPd_3$ and Cu_3Pd nanozymes. Furthermore, the atomic ratio of Cu/Pd in Cu–Pd bimetallic nanozymes is qualitatively verified by the EDS mapping, which are 1:3.4 for $CuPd_3$ and 3.4:1 for Cu_3Pd nanozyme (Fig. S6d&e).

Besides the elemental components measurement, the X-ray photoelectron spectroscopy (XPS) was performed to further investigate the surface chemical composition of Pd and Cu–Pd bimetallic nanozymes. As shown in Figs. S7a–c, none peak is detected for Cu 2p spectrum, but the narrow-scan Pd 3d spectra exhibits characteristic high (343.2 eV) and low (337.8 eV) energy regions that assigning to the $3d_{3/2}$ and $3d_{5/2}$ regions. For $CuPd_3$ nanozyme, the Cu 2p spectra appears and is divided into two regions (high energy region of 952.3 eV and low energy region of 932.5 eV), which are attributed to $2p_{1/2}$ and $2p_{3/2}$ (Figs. S8a–c). Meanwhile, the divided regions of Pd 3d remain (Fig. S8c) similar with that of

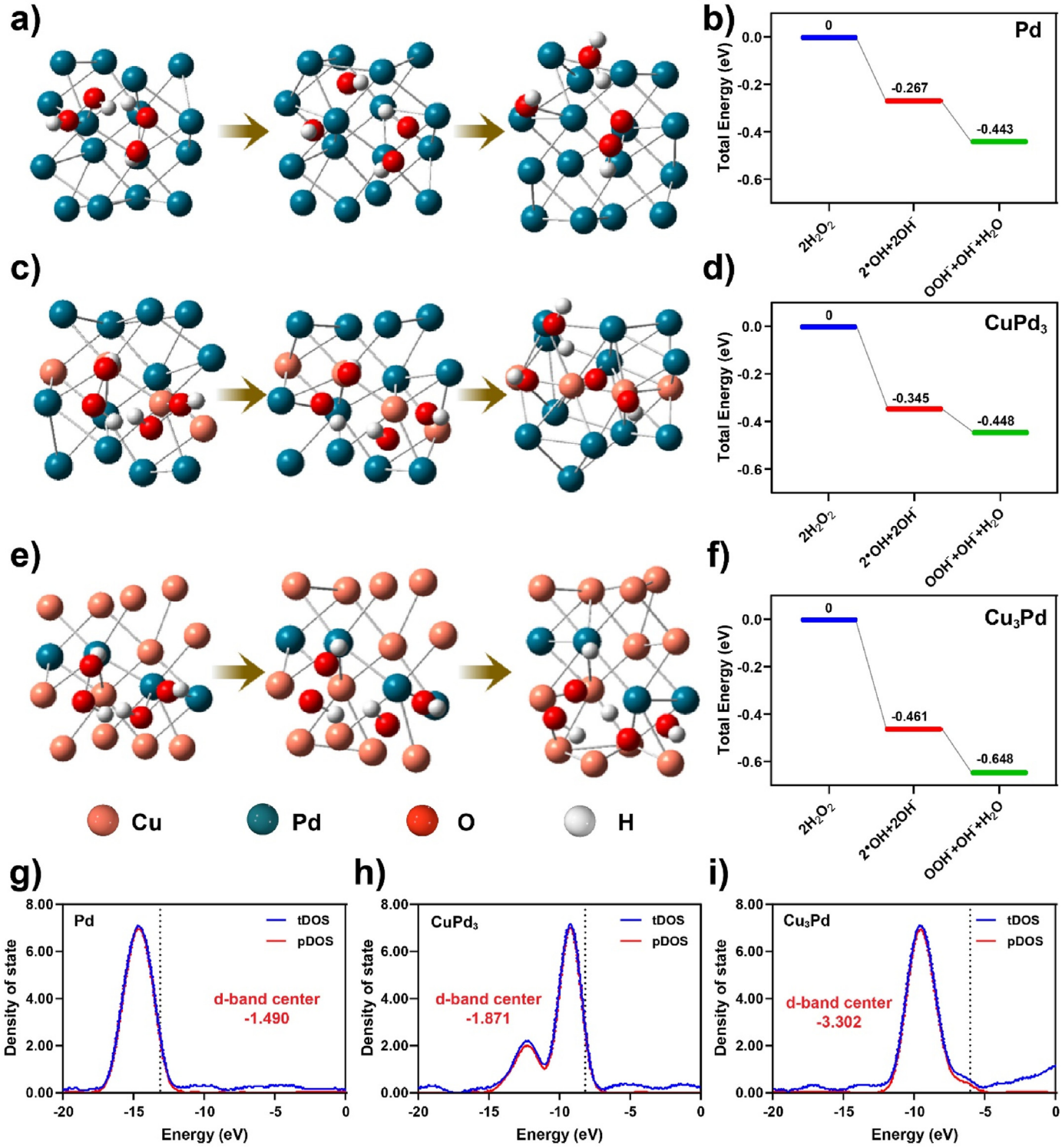

Fig. 5. Density Functional Theory (DFT) theoretical calculation for the Fenton-like efficiency of Cu–Pd bimetallic nanozymes. (a-f) The critical intermediate structures and corresponding total energy diagram of Fenton-like reaction path catalyzed by Pd (a, b), $CuPd_3$ (c, d) and Cu_3Pd (e, f) nanozymes. (g-i) The pDOS of d-band center analysis of Pd (g), $CuPd_3$ (h) and Cu_3Pd (i) nanozymes.

Pd nanozyme. With the increase of Cu amount, Cu_3Pd nanozyme exhibits more obvious Cu 2p peak in XPS survey spectra (Fig. S9a&b). Importantly, the peaks of narrow-scan Cu 2p spectra at Cu $2p_{3/2}$ shows the Cu(0) (931.9 eV)/Cu(I) (933.5 eV) species (Fig. S9b), indicating the partial Cu oxidation on the surface. The narrow-scan Pd 3d spectra of Cu_3Pd nanozyme is similar with that of $CuPd_3$ nanozyme (Fig. S9c), revealing the similar atomic state. Besides, the zero-valent metal peaks for the Cu 2p spectra in both $CuPd_3$ and Cu_3Pd nanozymes and Pd 3d spectra in all samples further confirming the homogenous alloying of Cu–Pd bimetallic nanozymes [16]. Based on above results, we speculate that both Cu and Pd atom are kinetically trapped in bimetallic lattice, as shown in Fig. 2g. Because the thermodynamic equilibrium state eliminates the phase segregation of Cu or Pd, homogeneity of Cu–Pd bimetallic nanozymes is obtained during the coreduction process, which has been verified by the AC-HAADF-STEM images.

3.2. XAS measurements for coordination structure

For further authenticating the kinetically trapped structure in Fig. 2g, X-ray absorption spectroscopy (XAS) was performed to investigate the precise coordination structure of the Cu–Pd bimetallic nanozymes. The Cu K-edge X-ray absorption near-edge structure (XANES) of both $CuPd_3$ (Fig. 3a) and Cu_3Pd (Fig. 3b) bimetallic nanozymes exhibit that the pre-edge peaks are located close to Cu-foil and far away from CuPc, indicating that the average valence of Cu in both $CuPd_3$ and Cu_3Pd nanozymes is Cu(0), which is consistent with the results of XPS spectra. Furthermore, the κ^3-weighted Fourier-transformed extended X-ray absorption fine structure spectra (FT-EXAFS) of both $CuPd_3$ (Fig. 3c) and Cu_3Pd (Fig. 3d) bimetallic nanozymes show that the major peak locates at about 2.25 Å, which means that the existence of Cu atom in lattice is not single-atom state. That is also verified by none significant peaks appear at about 1.56 Å as that in CuPc. Furthermore, the wavelet transform (WT) of the EXAFS plot (Fig. 3e&f) is employed to examine the atomic configuration via the information of κ- and R-spaces. As shown in Fig. 3e, both the centers of $CuPd_3$ nanozyme and Cu-foil are located at κ-space (about 7.95 $Å^{-1}$) and R-space (about 2.25 Å), which are attributed by the Cu–Cu scattering signal [17,18]. The WT image of CuPc presents a center at κ-space (about 6.25 $Å^{-1}$) and R-space (about 1.02 Å), revealing the typical signal of Cu–N coordinated center. In contrast to the WT image of Cu-foil and CuPc, it can be concluded that the Cu atoms in $CuPd_3$ nanozyme are Cu–Cu pair, a form of miscible bimetallic phase. Similarly, the WT-EXAFS of Cu_3Pd nanozyme (Fig. 3f) shows an average bond distance of 2.26 Å, indicating the typical Cu–Cu pair. All of the results confirm the as-speculated homogenously alloyed atomic arrangement structure of Cu–Pd bimetallic nanozymes (Fig. 2g).

3.3. Fenton-like activity evaluation of Pd and Cu–Pd bimetallic nanozymes

The Fenton-like reaction activity of as-synthesized Pd and Cu–Pd bimetallic nanozymes were systematically explored by 3,3′,5,5′-tetramethylbenzidine (TMB) colorimetric assays. The TMB could be efficiently catalyzed into oxidized TMB (oxTMB) by the Fenton-like reaction products (hydroxide racial: •OH) and generated oxTMB exhibits a characteristic absorption peak at about 652 nm, which is proportional to the amount of •OH [19]. Firstly, the Fenton-like reaction kinetics of Pd and Cu–Pd bimetallic nanozymes was investigated with various concentrations (Fig. 4a–c). As shown in Fig. 4a, although Pd nanozyme exhibits weak catalytic activity below 200 μg/mL, time-dependent oxTMB accumulation under 500 μg/mL shows significant enhancement, indicating the possible Fenton-like reaction catalyzed by Pd nanozyme. Compared with Pd nanozyme, $CuPd_3$ nanozyme reveals efficient catalytic activity (Fig. 4b). All the substrates (TMB/H_2O_2) were consumed by 200 μg/mL $CuPd_3$ nanozyme within about 20,000 s. And when the concentration was increased to 500 μg/mL, the reaction time would shorten to 11,000 s. Surprisingly, Cu_3Pd nanozyme presents highest Fenton-like efficiency for the reaction time is only about 8000 s with low concentration of 100 μg/mL (Fig. 4c). Meanwhile, the kinetic curve of Pd and Cu–Pd bimetallic nanozymes with same concentration (200 μg/mL) further clearly confirms the results that the introduction of Cu will efficiently optimize the Fenton-like reaction performance of Cu–Pd bimetallic nanozymes (Fig. 4d). Meanwhile, Electron spin resonance (ESR) was applied to detect the hydroxide radical trapped by 5,5-dimethyl-1--pyrroline N-oxide (DMPO) in aqueous solution. Compared with alone H_2O_2 group, no significant OH yield is detected for Pd + H_2O_2 group with concentration of 10 μg/mL (Fig. 4e). However, the strongly characteristic ESR spectra of spin adduct DMPO/OH are observed in both $CuPd_3$ + H_2O_2 and Cu_3Pd + H_2O_2 groups, indicating the successful generation of OH via Fenton-like reaction. Meanwhile, Cu_3Pd + H_2O_2 group exhibits the strongest peak intensity compared with Pd and $CuPd_3$, which is consistent with the results of kinetics assay. UV–vis absorbance value at 652 nm of TMB/H_2O_2 solutions after incubation with Cu–Pd bimetallic nanozymes (200, 150, 100, 50 μg/mL) for 1.5 h (Fig. 4f) demonstrates the concentration-dependent catalysis process and enhancement of Fenton-like efficiency via Cu-introduction, which is further confirmed by the UV–vis spectra in Fig. S10. And the photographs of TMB/H_2O_2 solutions after incubation with Cu–Pd bimetallic nanozymes for 1.5 h (Fig. 4g) intuitively illustrate the difference of reaction activity. The substrate concentration is one of the main variables to influence the activity of nanozyme [20,21]. Thus, the Fenton-like efficiency of Cu–Pd bimetallic nanozymes was evaluated in various H_2O_2 concentration system (Fig. 4h). With the increase of H_2O_2 concentration, all Cu–Pd bimetallic nanozymes present excellent catalytic response. However, compared with Pd, $CuPd_3$ and Cu_3Pd demonstrate faster reaction under higher H_2O_2 concentration system (Fig. S11). The catalytic kinetics were also measured to compare the catalytic activity of Pd and Cu–Pd bimetallic nanozymes in different substrate environment (Fig. 4i, Fig. S12). The results show that higher substrate concentration will bring faster reaction efficiency, indicating that substrate do not influence the activity of nanozymes. Meanwhile, the kinetics results under 40 μM H_2O_2 concentration increasingly confirms the enhanced Fenton-like property of Cu–Pd bimetallic nanozymes (Fig. S13). All above results reveal that as-synthesized Cu–Pd bimetallic nanozymes possess excellent Fenton-like reaction performance, and the reaction efficiency is effectively enhanced via increasing level of Cu.

3.4. DFT theoretical calculation for enhanced Fenton-like performance

The above optimized Fenton-like efficiency of Cu–Pd bimetallic nanozymes compared with Pd nanozyme inspires us to disclose the catalytic mechanism. Therefore, we performed the molecular dynamic simulation in a canonical ensemble (NVT) by using GFN2-XTB method in the CP2K package. Density of States (DOS) analysis has also been obtained by MULTIWFN 3.8 program, and d-band center was calculated to study the adsorption between the transition metal surface and H_2O_2. Fig. 5a–f shows the critical intermediate structures for the generation of ·OH from H_2O_2 catalyzed by Cu–Pd bimetallic nanozymes. The initial H_2O_2 molecular will absorb on the Pd and Cu–Pd bimetallic nanozymes and then dissociate into ·OH and OH^- homogeneously. Thereafter, one ·OH will react with H_2O_2 molecular to produce OOH^- and H_2O. Finally, the Cu–Pd bimetallic nanozymes will return to the original state via desorption of H_2O molecular [22]. Along this reaction routine, the total energy diagrams of Cu–Pd bimetallic nanozymes was calculated and

Table 1
The corresponding data of d-band center analysis from DFT theoretical calculation.

eV	Pd	$CuPd_3$	Cu_3Pd
tDOS	−13.679	−9.806	−8.828
pDOS	−14.633	−10.041	−9.366
HOMO level	−13.143	−8.170	−6.064
d-band center	−1.490	−1.871	−3.302

depicted in Fig. 5b,d,f. It is obviously that Cu_3Pd system presents the largest total energy decrease (0.648 eV) compared with that of $CuPd_3$ (0.448 eV) and Pd (0.443 eV), indicating the highest Fenton-like efficiency, which is consistent with previous experimental results. To further disclose catalytic mechanism, the partial density of states (pDOS) is explored to analyze the d-band of Cu–Pd bimetallic nanozymes. As shown in Fig. 5g–I, and Table 1, Pd nanozyme has a larger absolute pDOS value (14.633 eV) than that of $CuPd_3$ (10.041 eV) and Cu_3Pd (9.366 eV) bimetallic nanozymes, indicating the weaker interaction between Pd nanozyme with H_2O_2. Meanwhile, the order of d-band center is Cu_3Pd (−3.302 eV) < $CuPd_3$ (−1.871 eV) < Pd (−1.490 eV), demonstrating the easier absorption of H_2O_2 on the transition metal surface of Cu_3Pd then both $CuPd_3$ and Pd nanozymes. Our previous study has demonstrated that Pd atom has strong repulsive interaction to H atom in H_2O_2 due to

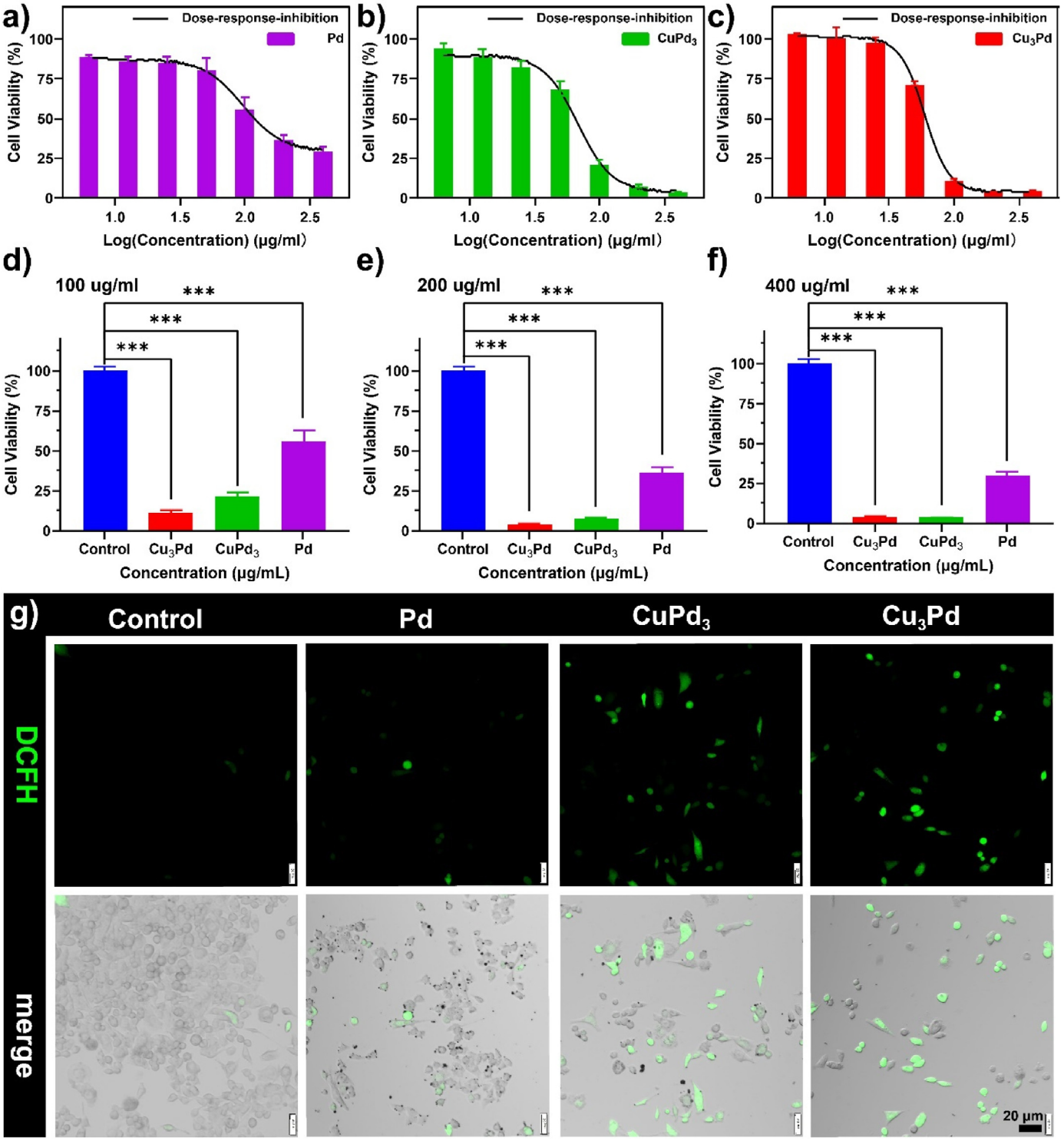

Fig. 6. *In vitro* cytotoxicity of Cu–Pd bimetallic nanozymes. (a-f) The cell viability of 4T1 cells after incubation with Pd and Cu–Pd bimetallic nanozymes (400, 200, 100, 50, 25, 12.5, 6.25, 0 μg/mL) for 24 h. (g) Fluorescent images of 4T1 cells after incubation with Pd and Cu–Pd bimetallic nanozymes (25 μg/mL) for 6 h and staining with DCFH-DA probe.

the electronic structure [23]. Herein, we speculate the easier absorption effect for $CuPd_3$ and Cu_3Pd is contributed by the optimized electronic structure of Cu compared with Pd nanozyme. Therefore, contributing by the optimized electronic structure by Cu to absorb H_2O_2 molecular and largest total energy decrease to produce ·OH, Cu_3Pd nanozyme displays highest Fenton-like efficiency than both $CuPd_3$ and Pd nanozymes.

3.5. In vitro evaluation of Fenton-like efficiency

As one of the tumor-specific treatments, chemodynamic therapy (CDT) mediated by both Fenton or Fenton-like reaction in tumor microenvironment (TME) has exhibited various advantages such as high selectivity, deep tissue penetration, and excellent sensitivity [24–26]. It is well known that the intracellular H_2O_2 level in tumor cells (about 50–100 μM) is higher than that of normal cells [27,28]. Therefore, the optimized Fenton-like efficiency of Cu–Pd bimetallic nanozymes inspire us to investigate *in vitro* antitumor effect. 4T1 murine mammary cancer cell line was chosen as model to coincubation with various concentrations of Pd and Cu–Pd bimetallic nanozymes (400, 200, 100, 50, 25, 12.5, 6.25, 0 μg/mL) for 24 h. The relative cell viabilities were evaluated by Cell Count Kit-8 (CCK-8) and the results were shown in Fig. 6a–f. Cu_3Pd (Fig. 6a), $CuPd_3$ (Fig. 6b), and Pd (Fig. 6c) nanozymes demonstrate the concentration-dependent cytotoxicity to 4T1 cells with corresponding IC50 value of 59.55 μg/mL, 68.18 μg/mL, and 95.82 μg/mL, respectively. As comparison, Cu_3Pd and $CuPd_3$ nanozymes have 1.6 and 1.4 folds cytotoxicity lower than Pd nanozymes, which is agreement with the kinetic results (Fig. 4). When incubation 4T1 cells with Cu_3Pd, $CuPd_3$, and Pd nanozymes with concentration of 100 μg/mL for 24 h, there are about 88.55%, 78.43%, and 44.15% cells were killed compared with Control group (Fig. 6d). And the cytotoxic difference among of them is remarkable due to the different Fenton-like efficiency. Once the concentration raises to above 200 μg/mL, practically all cells are unable to survival in both Cu_3Pd and $CuPd_3$ group (Fig. 6e), indicating the optimized Fenton-like performance in tumor microenvironment. It is notable that 29.75% of cells are still alive even incubating with 400 μg/mL Pd nanozymes, demonstrating the low biocatalytic performance and also good biocompatibility (Fig. 6f). Meanwhile, the biocompatibility of as-synthesized Pd and Cu–Pd bimetallic nanozymes were evaluated on mouse fibroblast cell line (L929), and the results (Fig. S14) show that few toxicities are observed even under 400 μg/mL nanozyme treatment. Furthermore, to verify the Fenton-like reaction catalyzed by Cu–Pd bimetallic nanozymes in 4T1 cells, 2′-7′dichlorofluorescin diacetate (DCFH-DA) which is a cell-permeant reagent fluorogenic dye that tests peroxyl, hydroxyl, and other ROS activity was employed to intuitively evaluate the generated ·OH [29]. After incubation with Cu–Pd bimetallic nanozymes (25 μg/mL) for 6 h, a few green signals are detected in Pd group compared with Control group (Fig. 6g, Fig. S15), indicating the successful generation of ·OH. Both $CuPd_3$ and Cu_3Pd groups exhibit obviously enhanced green signal, demonstrating higher ·OH level contributed by the enhanced Fenton-like efficiency, which is consistent with cell viability results. It is well-known that higher ·OH generation will cause the intracellular oxidative stress, which then upregulate the GSSG level [29]. It is clear that Cu–Pd bimetallic nanozymes treated 4T1 cells produce higher GSSG level compared with Pd nanozyme treated group (Fig. S16), which confirms the higher level of ·OH. All above results reveal the optimized Fenton-like efficiency of Cu–Pd bimetallic nanozymes compared with Pd nanozymes and great potential as agents for cancer chemodynamic treatment.

4. Conclusions

In summary, we presented a one-step coreduction strategy to prepare the miscible Cu–Pd bimetallic nanozymes with controllable shape and homogeneously alloyed structure to avoid the immiscibility and heterogeneity. The homogeneity is systematically explored through HRTEM, AC-HAADF-STEM with sub-Angstrom resolution, XPS, and XAS. Wavelet Transform images at the Cu-edge clearly demonstrate the homogenously alloyed structure of Cu–Pd bimetallic nanozymes via the κ-space and R-space. TMB colorimetric assays exhibit homogeneous introduction of Cu successfully endows Cu–Pd bimetallic nanozymes with enhanced Fenton-like efficiency, especially for Cu_3Pd nanozymes. Further density functional theory (DFT) theoretical calculation reveals that Cu–Pd bimetallic nanozymes exhibit smaller d-band center compared with Pd nanozymes. Easier adsorption of H_2O_2 molecular contributed by the electronic structure of Cu significantly accelerate the catalytic process together with the strong repulsive interaction between H atom and Pd atom. *In vitro* cytotoxicity and intracellular ROS generation performance are evaluated to reveal the potential for *in vivo* biocatalysis. The strategy to construct kinetically miscible Cu–Pd bimetallic nanozymes will guide the development of bimetallic catalysts with excellent Fenton-like efficiency for biocatalytic nanomedicine.

Credit author statement

Wensheng Xie: Conceptualization, Methodology, Investigation, Writing - review & editing. **Genpei Zhang**: Methodology, Calculation, Validation. **Zhenhu Guo**: Methodology, Investigation, Validation. **Hongye Huang**: Methodology, Investigation, Validation. **Jielin Ye**: Methodology, Investigation, Validation. **Xiaohan Gao**: Methodology, Investigation, Validation. **Kai Yue**: Writing - review & editing. **Yen Wei**: Conceptualization, Supervision, Writing - review & editing. **Lingyun Zhao**: Conceptualization, Supervision, Writing - review & editing.

Declaration of competing interest

The authors declare that they have no known competing financial interests or personal relationships that could have appeared to influence the work reported in this paper.

Acknowledgements

This work was supported by the National Natural Science Foundation of China (Nos. 81671829, 21788102, and 51971116), China.

Appendix A. Supplementary data

Supplementary data to this article can be found online at https://doi.org/10.1016/j.mtbio.2022.100411.

References

[1] S. Soled, Science 350 (2015) 1171–1172.
[2] K.D. Gilroy, A. Ruditskiy, H.-C. Peng, D. Qin, Y. Xia, Chem. Rev. 116 (2016) 10414–10472.
[3] D. Wang, Y. Li, Adv. Mater. 23 (2011) 1044–1060.
[4] G. Chen, N. Zou, B. Chen, J.B. Sambur, E. Choudhary, P. Chen, ACS Cent. Sci. 3 (2017) 1189–1197.
[5] C. Yang, B.H. Ko, S. Hwang, Z. Liu, Y. Yao, W. Luc, M. Cui, A.S. Malkani, T. Li, X. Wang, J. Dai, B. Xu, G. Wang, D. Su, F. Jiao, L. Hu, Sci. Adv. 6 (2020), eaaz6844.
[6] D. Kim, J. Resasco, Y. Yu, A.M. Asiri, P. Yang, Nat. Commun. 5 (2014) 4948.
[7] A. Wong, Q. Liu, S. Griffin, A. Nicholls, J.R. Regalbuto, Science 358 (2017) 1427–1430.
[8] W. Xie, Z. Guo, F. Gao, Q. Gao, D. Wang, B. Liaw, Q. Cai, X. Sun, X. Wang, L. Zhao, Theranostics 8 (2018) 3284–3307.
[9] M. Sankar, N. Dimitratos, P.J. Miedziak, P.P. Wells, C.J. Kiely, G.J. Hutchings, Chem. Soc. Rev. 41 (2012) 8099–8139.
[10] U. Aslam, S. Linic, Chem. Mater. 28 (2016) 8289–8295.
[11] K.A. Kane, A.C. Reber, S.N. Khanna, M.F. Bertino, Prog. Nat. Sci. 28 (2018) 456–463.
[12] U. Aslam, S. Chavez, S. Linic, Nat. Nanotechnol. 12 (2017) 1000–1005.
[13] B. Zhao, P. Liu, S. Li, H. Shi, X. Jia, Q. Wang, F. Yang, Z. Song, C. Guo, J. Hu, Z. Chen, X. Yan, X. Ma, Appl. Catal., B 278 (2020), 119307.
[14] V. Mukundan, J. Yin, P. Joseph, J. Luo, S. Shan, D.N. Zakharov, C.-J. Zhong, O. Malis, Sci. Technol. Adv. Mater. 15 (2014), 025002.
[15] E. Bruno, B. Ginatempo, E. Sandro Giuliano, Phys. Rev. B 63 (2001), 174107.
[16] Q. Li, L. Wu, G. Wu, D. Su, H. Lv, S. Zhang, W. Zhu, A. Casimir, H. Zhu, A. Mendoza-Garcia, S. Sun, Nano Lett. 15 (2015) 2468–2473.

[17] I.A. Pankin, A. Martini, K.A. Lomachenko, A.V. Soldatov, S. Bordiga, E. Borfecchia, Catal. Today 345 (2020) 125–135.
[18] Y. Ji, Z. Chen, R. Wei, C. Yang, Y. Wang, J. Xu, H. Zhang, A. Guan, J. Chen, T.-K. Sham, J. Luo, Y. Yang, X. Xu, G. Zheng, Nat. Catal. 5 (2022) 251–258.
[19] W. Xie, J. Lu, Z. Guo, X. Guo, Y. Chi, J. Ye, J. Zhang, W. Xu, L. Zhao, Y. Wei, Nano Res. 15 (2022) 2244–2253.
[20] Q.-Q. Wang, S. Gonell, S.H.A.M. Leenders, M. Dürr, I. Ivanović-Burmazović, J.N.H. Reek, Nat. Chem. 8 (2016) 225–230.
[21] C. Hu, Y. Bai, M. Hou, Y. Wang, L. Wang, X. Cao, C.-W. Chan, H. Sun, W. Li, J. Ge, K. Ren, Sci. Adv. 6 (2020), eaax5785.
[22] S. Cao, Z. Zhao, Y. Zheng, Z. Wu, T. Ma, B. Zhu, C. Yang, X. Xiang, L. Ma, X. Han, Y. Wang, Q. Guo, L. Qiu, C. Cheng, Adv. Mater. (2022), 2200255 n/a.
[23] W. Xie, G. Zhang, Z. Guo, J. Lu, J. Ye, W. Xu, X. Gao, K. Yue, Y. Wei, L. Zhao, Adv. Funct. Mater. 32 (2022), 2107518.
[24] S. Li, P. Jiang, F. Jiang, Y. Liu, Adv. Funct. Mater. 31 (2021), 2100243.
[25] Q. Tian, F. Xue, Y. Wang, Y. Cheng, L. An, S. Yang, X. Chen, G. Huang, Nano Today 39 (2021), 101162.
[26] W. Xie, J. Ye, Z. Guo, J. Lu, X. Gao, Y. Wei, L. Zhao, ACS Appl. Mater. Interfaces 14 (2022) 21931–21944.
[27] C. Liu, Y. Cao, Y. Cheng, D. Wang, T. Xu, L. Su, X. Zhang, H. Dong, Nat. Commun. 11 (2020) 1735.
[28] B. Halliwell, M.V. Clement, L.H. Long, FEBS (Fed. Eur. Biochem. Soc.) Lett. 486 (2000) 10–13.
[29] W. Xie, J. Ye, Z. Guo, J. Lu, W. Xu, X. Gao, H. Huang, R. Hu, L. Mao, Y. Wei, L. Zhao, Chem. Eng. J. 438 (2022), 135372.